ORIGINAL RESEARCH ARTICLE

Effect of Processing and Anisotropy on the Morphology and Performance of the $Pr_{2/3}Cu_3Ti_4O_{12}$ (PCTO) Dielectric Material

N.B. SINGH, CHING HUA SU, BRIAN M. CULLUM, FOW-SEN CHOA, BRADLEY R. ARNOLD, and K.D. MANDAL

The aim of the present study was to investigate effects of processing at the low and high temperatures on the anisotropy, microstructure; and electrical properties of $Pr_{2/3}Cu_3Ti_4O_{12}$ (PCTO) dielectric materials. The experimental approach involved the synthesis, sintering and grain growth at two temperatures, followed by analysis of the resulting materials, their morphology, capacitance, and resistivity. Synthesis was performed using oxide source materials in stoichiometric ratio and grain growth was monitored for the ceramics processed at 900 °C and 1000 °C. Morphological results indicated that grain growth occurs *via* the channeling mechanism and subsequent grain merging. High temperature processing showed that stabilized grains are rich in copper and stabilize into faceted grains due to changes in interface energy anisotropy due to the higher copper concentration. Electrical characterization of the materials processed at 1000 °C indicates that with copper migration from the grain boundaries to grains, the capacitance of the composite increased, while the resistivity is decreased. Additionally, difference in the anisotropy due to increased concentration of copper in grains produces facetted surfaces and screw dislocation steps on the facets.

https://doi.org/10.1007/s11661-025-07856-8

I. BACKGROUND

There have been continuous efforts to understand the mechanism by which perovskite materials exhibit high dielectric values since the demonstration of the high dielectric constant in calcium copper titanate, $CaCu_3Ti_4O_{12}$ (CCTO) by Subramanian and his co-workers.[1] Several articles[2–4] have discussed synthesis processes and mechanisms for their high dielectric constant. The mechanisms,[5–7] known as the solid dielectric model and the internal grain boundary-based model, have been suggested to explain the high dielectric constant in perovskites. Among these mechanisms, the internal grain boundary barrier layer capacitance (IBLC) model is widely accepted for these large dielectric values. Although perovskites were discovered almost six decades ago[8] and their structures were described as $ACu_3Ti_4O_{12}$ (A = Ca, Ba, Sr), a variety of pure and doped oxides with complex structures have been developed with different synthetic routes including: solid-state, semi-wet and wet methods,[9–14] resulting in ideal ceramic materials for dielectric, magnetic and ferroelectric applications. Of these different perovskites, calcium-based materials have attracted much attention due to their environmentally friendly nature as opposed to lead and other heavy metals. For this reason, calcium copper titanate, $CaCu_3Ti_4O_{12}$ (CCTO) which belongs to the $ACu_3Ti_4O_{12}$ family, and with pseudo-cubic perovskite structure was a logical and favorable choice for several numerous investigations.[15–18] With colossal dielectric constant reported, up to ~ 10^5, and stability in the temperature range of 100 K to 600 K[18] the material represents a potentially important breakthrough for many different industrial applications. Unfortunately, the inability to reproducibly fabricate CCTO materials with high resistivity and randomly achieved high dielectric values have been a hurdle to their wide-spread adoption as materials for industrial components and systems. To achieve homogeneous materials with reduced sintering time and temperatures, several alternative synthetic processes have been

N.B. SINGH and FOW-SEN CHOA are with the Department of Chemistry and Biochemistry, and Computer Science and Electrical Engineering, University of Maryland, Baltimore County, Baltimore, MD 21250. Contact e-mail: singna@umbc.edu CHING HUA SU is with the NASA Marshall Space Flight Center, Huntsville, AL 35812. BRIAN M. CULLUM and BRADLEY R. ARNOLD are with the Department of Chemistry and Biochemistry, University of Maryland, Baltimore County, Baltimore, MD 21250. K.D. MANDAL is with the Indian Institute of Technology, Banaras Hindu University Varanasi, Varanasi, Uttar Pradesh 22105, India.
Manuscript submitted April 25, 2024; accepted June 6, 2025.
Article published online June 26, 2025

proposed.[3,14–16] Doping and substitution tried[19–23] to increase resistivity. The lead doping and substitution using isovalent and non-isovalent ions for Ca^{2+} and Cu^{+} for the CCTO ceramic material did not produce materials with any significant increase in resistivity.

In the present paper, we investigate $Pr_{2/3}Cu_3Ti_4O_{12}$ (PCTO) as a potential alternative ceramic material to achieve the desired physical and electrical properties as well as different synthetic processes to explore reasons for previous differences in the dielectric constants of perovskite materials from batch to batch. Studies on a variety of optical and electronic bulk, micro, and nano thin films and crystals have shown that morphology often controls performance. This work focuses on morphology, mechanisms of grain growth, and the effect of anisotropy.[24] To understand the morphological evolution, grain growth, and variation of copper concentrations in boundaries and grains, samples were processed at two different temperatures 900 °C and 1000 °C for the grain growth.

II. EXPERIMENTAL METHODS

The present experimental approach utilizes parent materials of oxides/carbonates and develops large grains by sintering and grain growth with and without flux. Along with the evolution of microstructure from a transient state to a stable morphology, measurements of dielectric constant and resistivity were also made for the PCTO material.

A. *Sample Preparation*

The samples were prepared from the parent components Pr_2O_3, CaO, Cu and TiO_2 supplied by Aldrich Chemical Company. The purity of Pr_2O_3 and CaO was listed as 99.95 pct, CuO was 99.9995 pct and TiO_2 was 99.9 pct. Particle sizes were in the ranges 20 to 100 nm. For a typical experiment 5 to 6 g of powder were used. Stoichiometric amounts of each component were thoroughly mixed and uniaxially pressed to 5500 to 7000 lb/in.^{2} pressure to make the pellets of the material.

B. *Sintering and Grain Growth*

Pellets were placed in a furnace at 200 °C overnight. Then samples were placed in a porcelain boat and the furnace temperature was raised to 900 °C and 1000 °C and processed for 96 hours to allow for grain growth.

C. *Microstructural Studies*

Details of the microstructure of the synthesized and annealed pellets were characterized by the scanning electron microscope NOVA NANOSEM 450. The voltage used in the study was in the range of 5 to 10 kV energy for studying microstructure.

D. *Electrical Characterization*

Details of the electrical characterization measurement system employing parallel polished surfaces of pellets have been described in detail previously.[15–20] The surfaces of the pellets were prepared to achieve good quality polished surfaces with fine sandpapers followed by cloth-based pads and surfaces were cleaned using acetone. The silver paste was used as the electrode contact to determine the capacitance and resistance of the pellets. Both the gold and silver electrodes were found to be stable electrode materials on the pellets. The capacitances and resistances were measured using a Hewlett Packard 4263A LCR meter. For the determination of the dielectric constant from the measured capacitance, we used the standard equation for parallel plates given as follows:

$$C = \varepsilon\varepsilon_o A/d,$$

where ε is the dielectric constant of the material, $\varepsilon_o = 8.854 \times 10^{-12}$, C is the measured capacitance, A is the overlapping surface area of the plates, and d is the thickness of the pellet. The dielectric constant and resistivity of bulk samples were inferred from the measurement of the complex impedance as a function of frequency from 100 Hz to 100,000 kHz at the bias voltage of 50 to 1000 mV. We synthesized identical size of pellets to compare the capacitance and resistance of

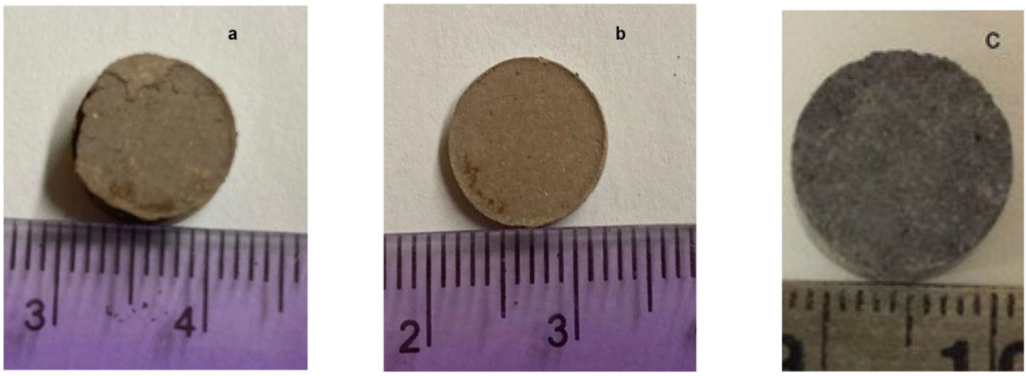

Fig. 1—(*a*) As synthesized PCTO pellet, (*b*) pellet processed at 900 °C for 96 hours and (*c*) processed pellet at 1000 °C (scale mm).

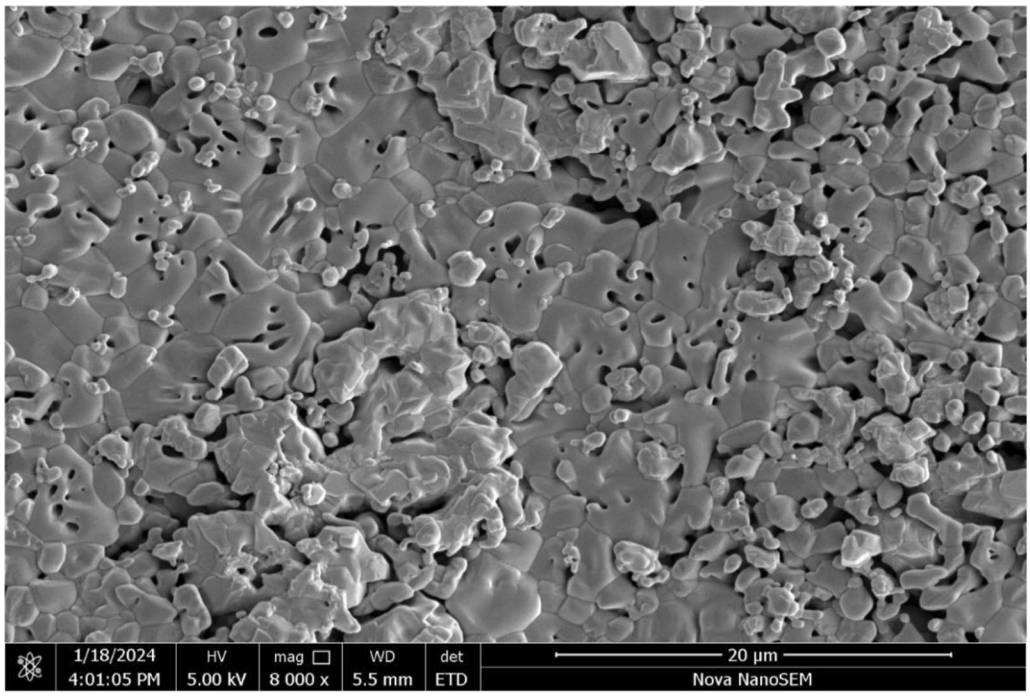

Fig. 2—Microstructures show elongated and non-faceted grains and unfilled gaps between grains. The dark spots show gaps between grains.

the PCTO ceramic processed at two different temperatures.

III. RESULTS AND DISCUSSION

As synthesized Figure 1(a), and processed typical samples are shown in Figures 1(b) and (c) respectively for the 900 °C, and 1000 °C annealing temperatures. Figure 1(c) shows that the sample processed at 1000 °C is darker than sample processed at 900 °C. Since the praseodymium oxide and titanium oxide compounds were white, and only the copper can change color, attention was paid to the copper concentration in the grain boundaries and semiconducting grains.

The dark color of the pellet processed at 1000 °C suggests that concentrations of the components and their structures/morphology could be different in the internal barrier layers due to the difference in the heat treatment. If the structures of internal barrier layers change, the corresponding overall microstructure will also be different, revealing that the processing temperature will control both the local grain shape and size.

A. *Microstructural Studies*

The microstructure and the concentration of the grains and grain boundaries were determined using a scanning electron microscope (SEM) and the electron energy dispersive X-ray spectroscopy (EDX) at high magnification. Since Schmidt *et al.*[5] previously indicated that most of the effects on IBL start to occur at annealing temperatures of 900 °C range, samples in this work were processed at either 900 °C or 1000 °C. Although the highest dielectric constant[18] in the perovskite CCTO and rectangular faceted microstructure were obtained by samples processed at 1120 °C, this study was focused using slightly lower temperatures to evaluate the temperature dependent microstructure evolution, transition and variations in the local component concentrations at the grain boundaries.

Figure 2 shows SEM images, revealing the morphology of pure PCTO processed for a period of 96 hours at 900 °C. Figure 3(a) shows a higher magnification image revealing the grain growth. The sample processed at 900 °C showed unstable morphology mostly with non-faceted structures across the sample. However, the observed morphology showed elongated grains and gaps between the grains for samples processed at 900 °C temperature.

Figures 3(a) and (b) show several morphologies, channels, gaps and merging of small grains into larger grains. To further elucidate the mechanism, high magnification microstructures were taken at two spots of the samples. It is clear from Figure 3(a) that grain growth occurred by neck formation, and engulfment of smaller grains into larger grains. Figure 3(b) shows stacking, merging and layering of smaller grains into the larger grains. The figure shows dominance of smaller grains on the top of larger grains and dissolution of these smaller grains into larger ones. As shown in Figure 3(b) bundles of 50 to 200 nm size grains merged and formed large grains (up to 500 to 1000 nm) and channels between grains. Figure 3(c) shows the combination of necking, channeling and merging into larger grains, and stacking of grains. Careful observations of the remaining small (25 to 100 nm) and large grains (500 to 2000 nm) both revealed very little if any indication of faceted grain in

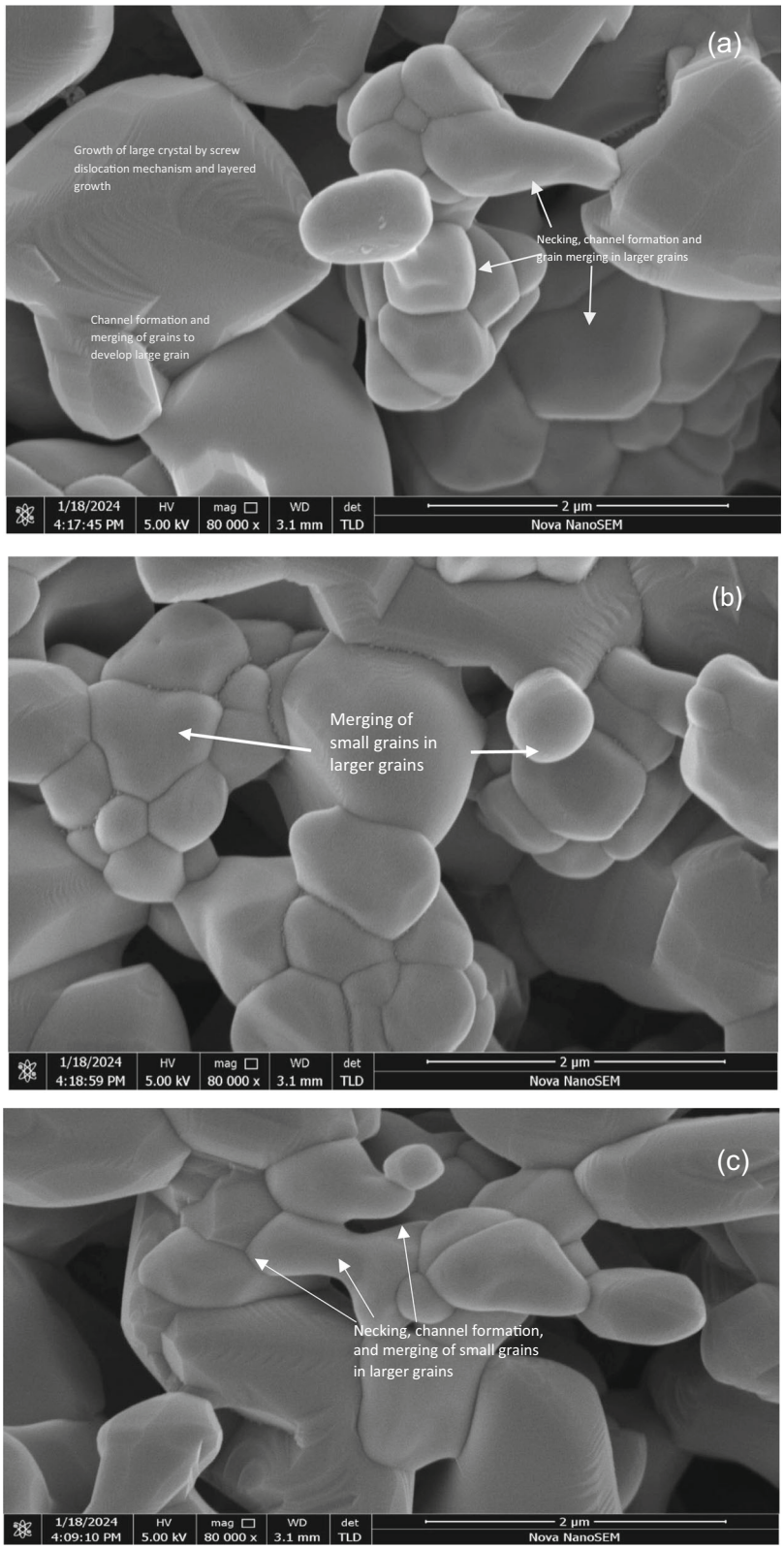

Fig. 3—(*a*) Necking and channel formation, (*b*) stacking and merging small grains into larger grains and (*c*) combination of formation of necking, channels and merger into larger grains and stacking in other areas than shown in (a).

PCTO processed at 900 °C temperature, revealing that for samples processed at 900 °C are meta stable and grain growth occurs mechanisms of necking, merging and channel formation during grain growth. These mechanisms can be easily discussed based on the sketch shown in Figures 4(a) and (b).

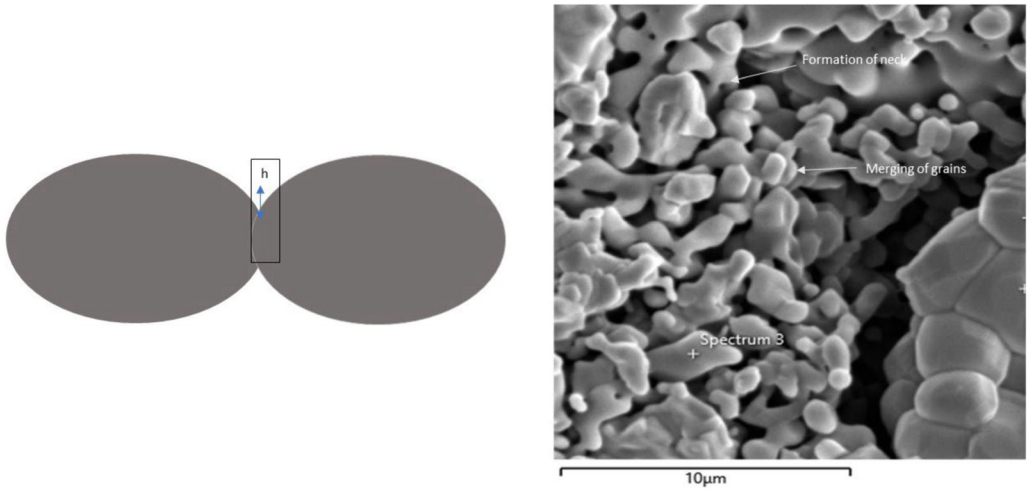

(a)

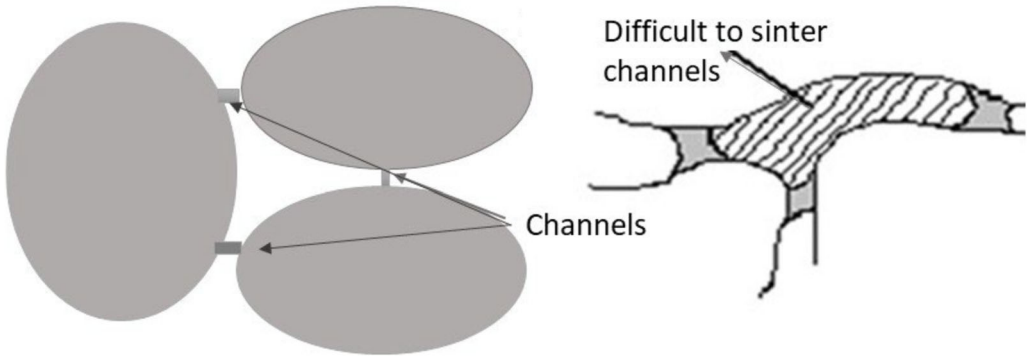

(b)

Fig. 4—(*a*) Figure shows sketch of two grains merging and formation of necks and observed actual necks and channels in PCTO processed at 900 °C and (*b*) shows sketch of neck and channel formation and area very difficult to sinter. The sizes of channels were up to a micrometer range.

Figure 4(a) shows a sketch of merging grains, and experimentally observed morphology with necks, channels and dissolution of smaller grains into a larger grain. As shown in the sketch, in an ideal spherical grain, the height d, radius of particles and surface area play a very important role. As shown in Figure 4(b), observed microstructures show that shapes are not perfectly spherical, and there is no uniformity in the radius. The role of parameters including surface energy, radius and grain shapes in coarsening and grain growth have been discussed in the past many decades[25–30] by several authors. The schematics of channels and areas difficult to sinter shown in Figure 4(b) are based on the observed morphology of PCTO shown in Figures 3(a) through (c). These channels and necks were extremely difficult to get filled during the growth. It was observed that around channels and necks, smaller grains on top of neighboring grains stacked up as shown in Figures 3(a) and (b). The observation of necking and channel formation were observed only in materials processed at lower temperatures (900 °C). Facets were formed in materials processed at higher temperatures as discussed in the following section.

Alternatively, samples processed at 1000 °C were much darker than samples processed at 900 °C, revealing a variation in the composition locally and changing morphology. Since the local composition differences at grain boundaries can dramatically affect the physical properties of a material, this color difference suggested the potential for different grain growth mechanisms and morphology. Upon examination under SEM (see Figures 5a and b), the presence of large facets on the individual grains are apparent.

Since the copper oxide has the lowest melting temperature among the various components used to synthesize the materials as well as a darker color, attention was focused on the variation of copper concentration in the grains and at the grain boundaries. Although electron dispersive X-ray spectroscopy does not provide definitive quantitative analyses, it was used to compare the relative concentrations of copper at the boundaries and within the individual grains for the samples

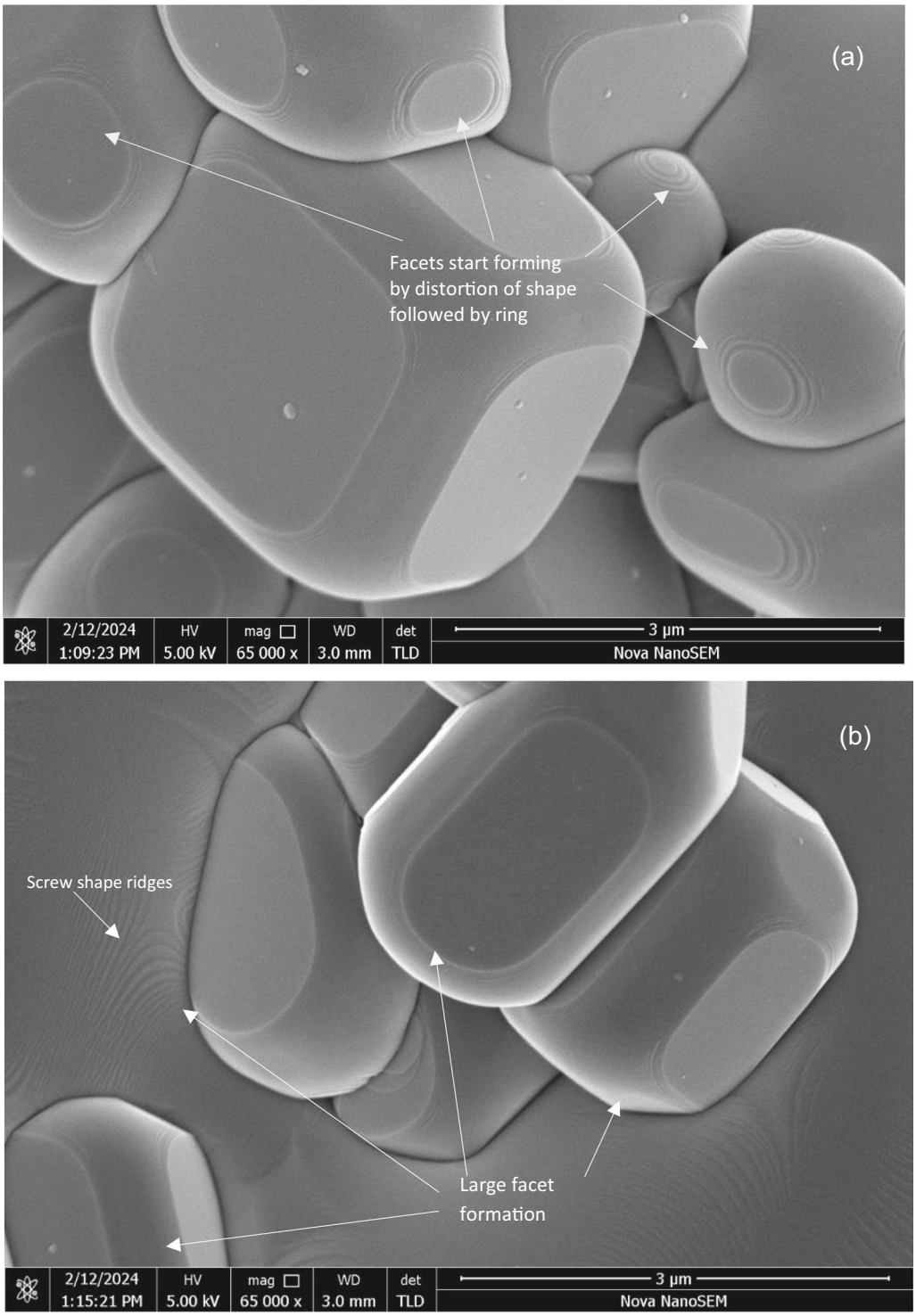

Fig. 5—(*a*) A combination of large facets and preformation of facets, and (*b*) shows area showing ring formation. As grains grew larger, rings were visible on grains.

processed at different temperatures. For the comparison, measurements were made in triplicate at each location on each sample and averaged together. For the samples that were processed at 900 °C, relative copper concentrations in the open areas between grains were found to be as high as 70 wt pct. However, in well-developed grains, the copper concentration was approximately 24 wt pct, suggesting that copper-rich melt is migrating from one part to another. Alternatively, in the case of samples processed at 1000 °C, the grains had very large relative concentrations of copper, compared to boundary areas. In these samples, the copper concentration of boundary varied between 0.3 and 5.4 wt pct and grains exhibiting concentrations of

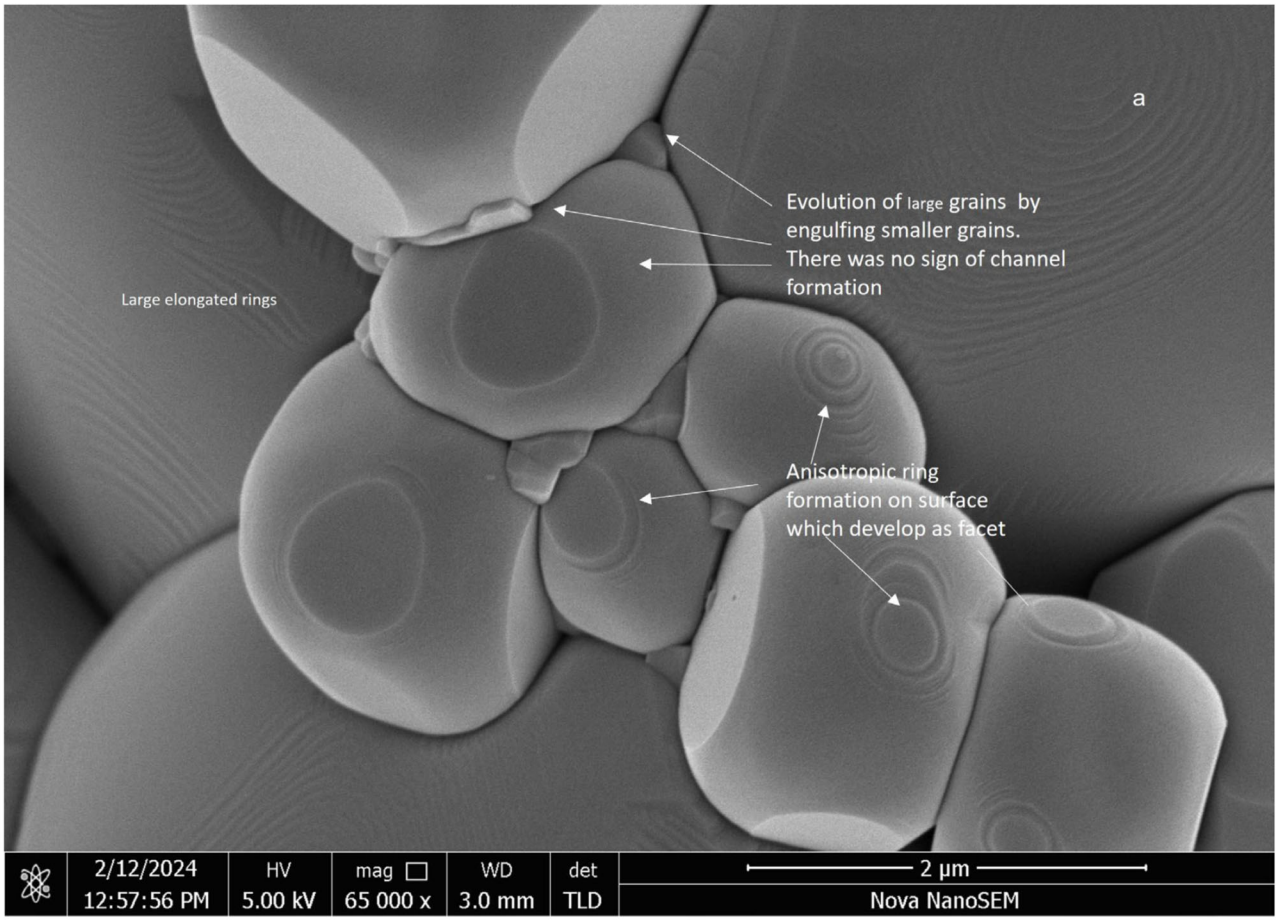

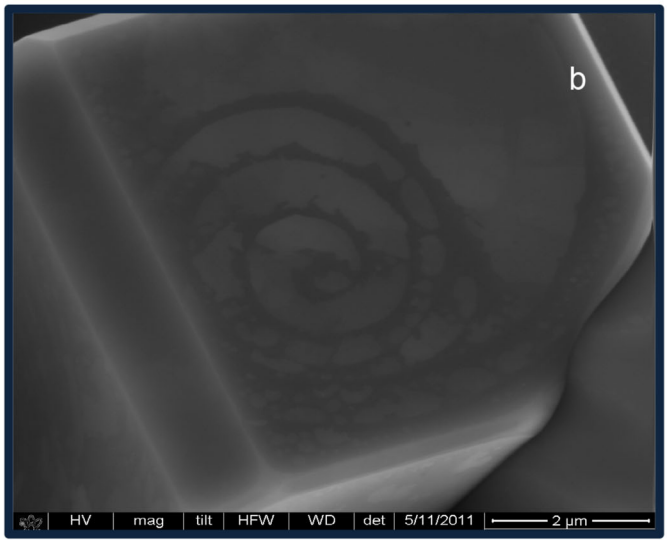

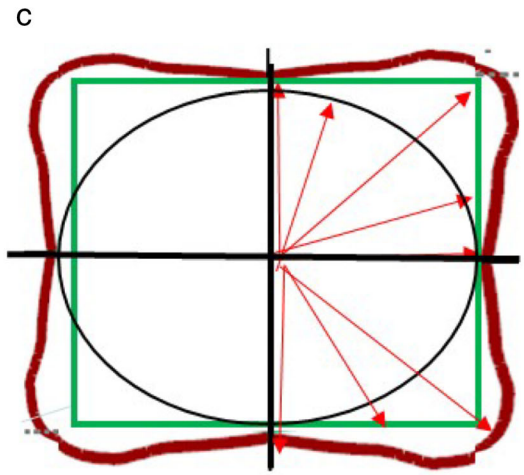

Fig. 6—(*a*) Faceted morphology with large arrays of rings on the faceted grains, (*b*) large step in the screw shape on the top of grains, and (*c*) surface energy shown by Wolff shape construct showing isotropic and anisotropic sketch. The isotropic and anisotropic shapes for transparent materials have been observed and discussed in details in Ref. [25] in details (Color figure online).

copper between 10 and 26 wt pct. Although it was difficult to focus the beam only on boundaries, since the grains merged with other grains leaving only small open spaces, measurement showed very clearly that grains in high temperature processed materials had significantly higher copper concentrations than their corresponding boundary areas. Furthermore, the concentration of copper-rich melt in the grain boundaries of samples processed at 900 °C was much larger compared to material processed at 1000 °C.

Figure 6(a) shows large arrays of rings developed before and during the formation of facets. After the facets formations these rings disappeared. In addition, to the facet formation, disappearance and merging of small grains were observed between neighboring large grains. Figure 6(b) shows that large steps in the screw shape formed on the surface of the well-developed faceted grain showing growth by the screw dislocation mechanism. This results in the Wolff construction for the energy function. In addition to the development of clear faceted grains in the samples processed at 1000 °C, SEM imaging of the samples reveals microstructure indicating a mechanism of facet formation. Figure 6(a) shows large arrays of rings developed before the formation of facets. There are also signs of screw shape large steps formed on the surface of the well-developed grain. This indicates possibility of screw dislocation mechanism to generate these surfaces, as opposed to melt and merge mechanisms of formation observed with the samples processed at 900 °C. This transition to faceted grains in samples processed at 1000 °C is extremely interesting and to our knowledge, the first-time rings were observed which facilitate the growth of facets. On some surfaces of the grains, the original rings do not completely disappear. The shape of these rings shows anisotropy, revealing a screw dislocation type growth of the surface.

These morphological transitions show that the variations of local copper concentrations as described earlier, in both of the processed materials (*i.e.*, 900 °C and 1000 °C samples) result in dramatically different structures. This can be explained with the Wolff shape-based surface energies in facets observed in PCTO processed at 1000 °C. Seto[24] has discussed in great detail with slightly different shapes than shown in Figure 6(c), how these structures are created. The Wolff shape construct for the energy function is shown by the green line (Figure 6c). Also in the same figure, surface energy is shown by the Wolff shape construct black line for the isotropic and red line for anisotropic shape. The surface structure of the crystal can be determined by first creating a polar plot shown by Seto[24] of the surface energy as a function of orientation, known as a gamma plot. By drawing vectors from the origin to every point on the gamma plot and then creating a tangent to each of these vectors, the resulting tangent surface determines the minimal energy shape or crystal structure and is known as the Wolff construct. Based on a large amount

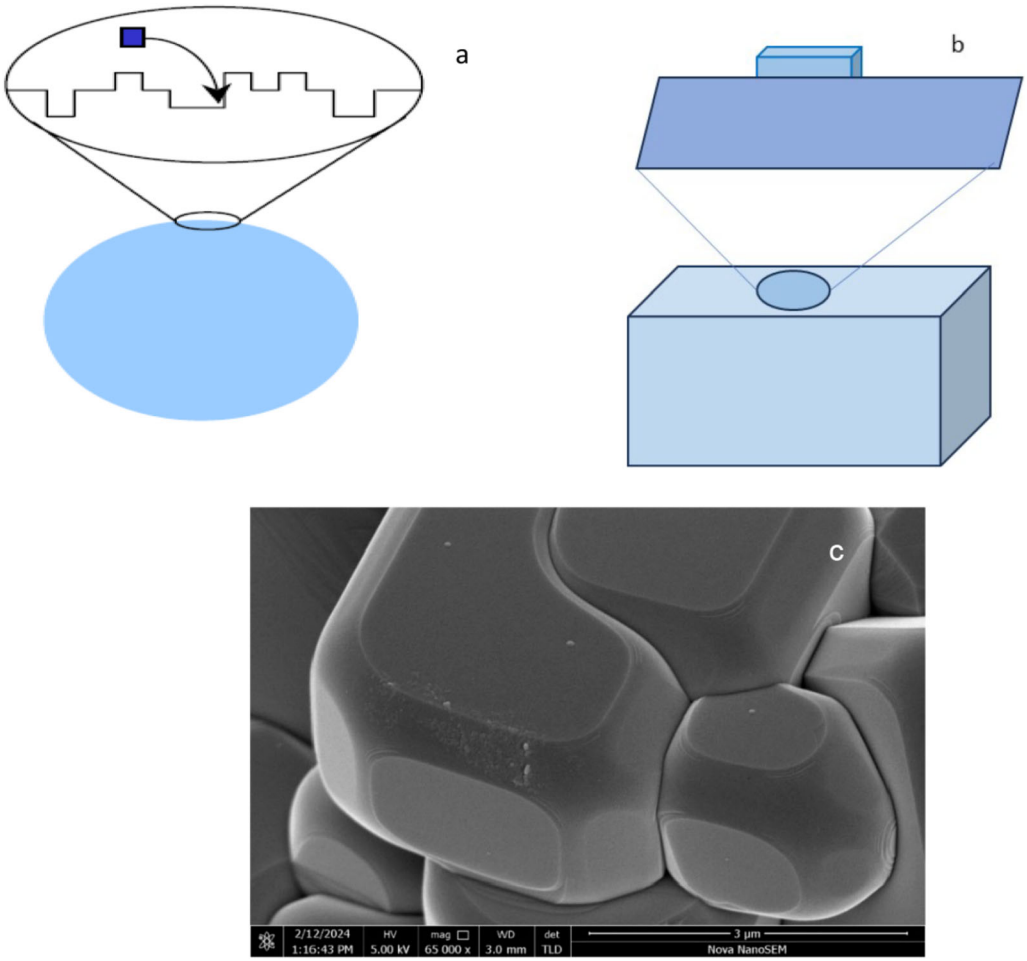

Fig. 7—(*a*) A rough surface with kinks that provide attachment and removal sites similar to that in Ref. [31] and (*b*) a flat facet with no preferential sites and (*c*) observed transition into faceted microstructures in PCTO ceramics.

of Wolff constructs theorized[26] over the years, Herring[27] described five possible types of equilibrium shapes for crystal structures, which explain the complex structures observed in this study for both temperatures. However, as a function of time at high temperature these structures change to more stable structures. As shown in Figure 5, PCTO processed at 1000 °C begins shaping as it starts coarsening. It is interesting to mention that in most of the perovskite materials researchers have observed,[18–20] faceted shaped grains obtained similar to observed for materials processed above 1100 °C. The grains start growing in the presence of Cu rich phases, which form small, segregated copper rich precipitates and these precipitates transform into shaped nuclei with rough rings on the surfaces. At some locations, solid–liquids materials were still present in the matrix which appeared as ring shaped nuclei. This is analogous to aspects related to the growth of a solid from a liquid, such as surface nucleation or spiral growth. The ring ultimately turns into a small flat surface. It shows that faceted crystals are formed after grains are developed with rough interfaces as shown in

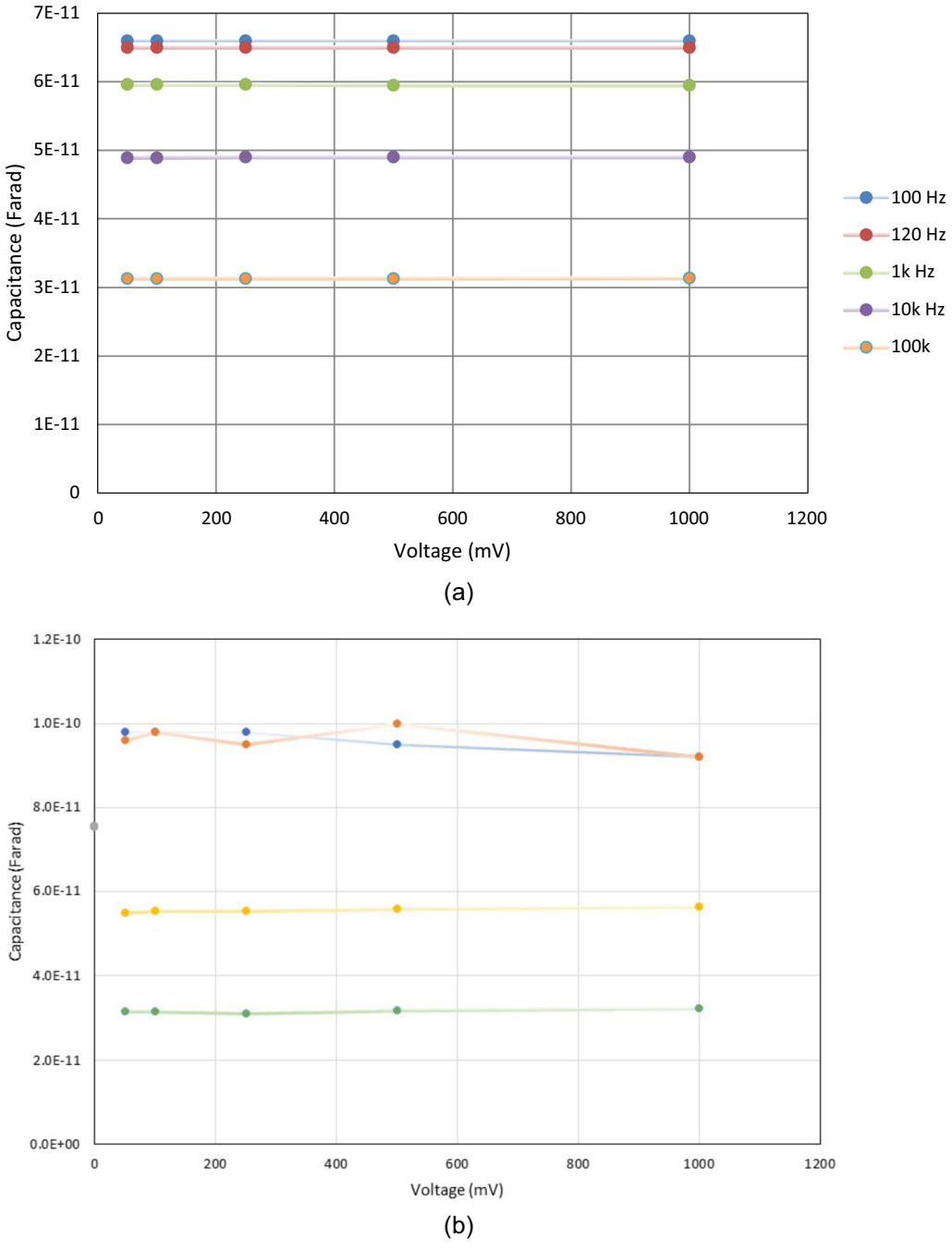

Fig. 8—(*a*) Capacitance of PCTO ceramic processed at 900 °C and (*b*) PCTO ceramic processed at 1000 °C for identical size parallel pellets (notations are same for both figures a and b).

Figure 5(a). Although it has been established that the driving force for coarsening is provided by excess interfacial free energy, the situation is simple for the case of isotropic interface energies and the resulting spherical crystals that are grown may be explained on the basis of classical theory[28,29] theory of coarsening, established by Lifshitz, Slyozov, and Wagner (LSW model), which assumes that each interface between a minority phase domain and the majority phase background is infinitely sharp (Figure 7).

The LSW model assumes that the coarsening phase is infinitely dilute and the average chemical potential surrounding each crystal is the same. In such crystals, the critical radius of the grain (r^*) can be given by the relationship $r^* = 2\gamma/\mu$, where γ is the surface energy per unit area μ is the chemical potential. In such cases, crystal of the size r^* neither shrinks nor grows. Grains larger than the critical radius r^*, grow while those smaller than r^* shrink. LSW theory has been reported to qualitatively agree with many experimental observations, but the details do not provide accurate quantitative results. As a result, a large number of papers have been published[30–36] that refine this model to account for various growth parameters. In the LSW model. No explanation of the occurrence of bimodal grain growth is provided in cases with anisotropic surface energies. Alternatively, some researchers have proposed that faceted grains can develop by the Ledge Coarsening Mechanism (LCM) in cases where the diffusion rate and the surface attachment rates are comparable. Shiflet *et al.*[31] proposed a ledge limited model of coarsening cubes where they assumed that the surfaces of the cubes migrated only by the ledge mechanism. Unfortunately, this again does not satisfactorily explain the morphologies observed in the microstructures observed in Figures 4 and 5 show that PCTO grains are not completely cubic in shape. One explanation may be that the ledge mechanism specifies that the interfaces have partially coherent steps on the surfaces. Their model is based on a situation where coarsening occurs only by particles attaching or detaching at surface ledge sites, which is different since our lower temperature morphology shows channel formation in addition to engulfment of smaller particles. Voorhees and colleagues[32–36] have developed Grain growth and grain translation in small crystals and extended modified Ostwald ripening of spheroidal particles in multicomponent alloys, some extremely careful direct observations of Glickman and colleagues[25] have demonstrated that practically there is always some anisotropy in the material. Although the mechanism of abnormal coarsening in anisotropic is complex and less understood, Voorhees has performed pioneering research using multicomponent materials[36] with anisotropy to highlight the mechanism for anisotropic materials. Since there on the interface energy anisotropy in multicomponent perovskites is lacking, it is extremely difficult to compare the growth of transition and multimode growth of crystals. Also, as observed on faceted grains signs of ridges and screw type steps show another complexity.

The effect of transition from non-equilibrium shapes at lower temperature to faceted structure due to copper deficient and copper rich composite is very significant. Although it is well established that microstructures control the properties, one of the aims of this study was to explore the reason why different investigators report observing different values of capacitance (dielectric constant) and resistance (resistivity). The details of dielectric constant, resistivity and loss will be presented in a future communication. However, for the identical samples processed, we observed that the intrinsic bulk capacitance and GB permittivity increased significantly (Figures 8 and 9) in materials processed at 900 °C and 1000 °C. Figures 8 and 9 show that higher capacitance and lower resistivity were accompanied by increased Cu segregation in materials processed at 1000 °C.

Most of the previous studies have been performed to determine the electrical measurements, and the mechanism of a high dielectric constant has been focused on capacitance and resistance. The transition observed here at lower temperature showed developments of final morphology and variation of composition variation in the metastable phases and variations in electrical properties. Among the three models proposed[5–7] to explain large capacitance, the nonstoichiometric redox model suggests a small amount of Ti^{4+} ions occupy the Cu-site when Cu^{2+} ions are partially reduced to Cu^{+} ions at high temperatures. When samples are cooled Cu^{+} ions are re oxidized to Cu^{2+} ions and the released electrons enter the Ti 3d conduction band giving rise to the bulk semi conductivity. The second model based on the Maxwell–Wagner–Sillars model[5] suggests that insulating grain boundaries and high dielectric constant occur when charge carriers accumulate at the interface of two materials with varying conductivities. When an electric field is applied, charge species move through grains and accumulate at grain boundaries, forming back-to-back Schottky barrier like diodes, and charge buildup leads to increased polarization and capacitance. The well accepted model of Sinclair *et al.*[7] known as Internal Barrier Layer Capacitance (IBLC) indicates that in the final processed perovskite the grains are semiconducting, and grain boundaries are insulating. In the IBLC model, one can assume that resistors correspond to the bulk and GB resistivity respectively, and the capacitance represents bulk and GB permittivity, respectively. Especially the significant difference in activation energy is a strong indicator of different charge transport mechanisms. The IBLC model[7] explains that permittivity drops when the mean electron conduction path is permitted by the applied alternating voltage and the signal decreases below the average grain size at increased frequency. The high frequency capacitance therefore is dominated by the conducting grains and the low frequency response by the insulating grain boundary contribution. Despite this IBLC model which explains most of the phenomena, such as differences in concentration, differences between GB and bulk in perovskite grains is still not fully understood or explained. The chemical changes due to possible Cu-gain in the PCTO grains and loss of copper in the boundary area for the materials processed at 1000 °C provide explanation for

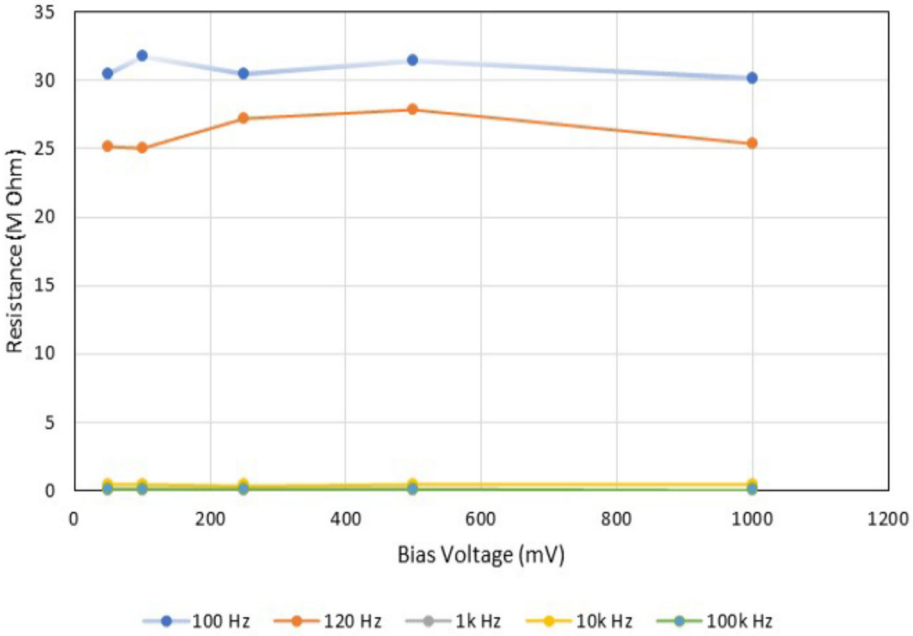

(a)

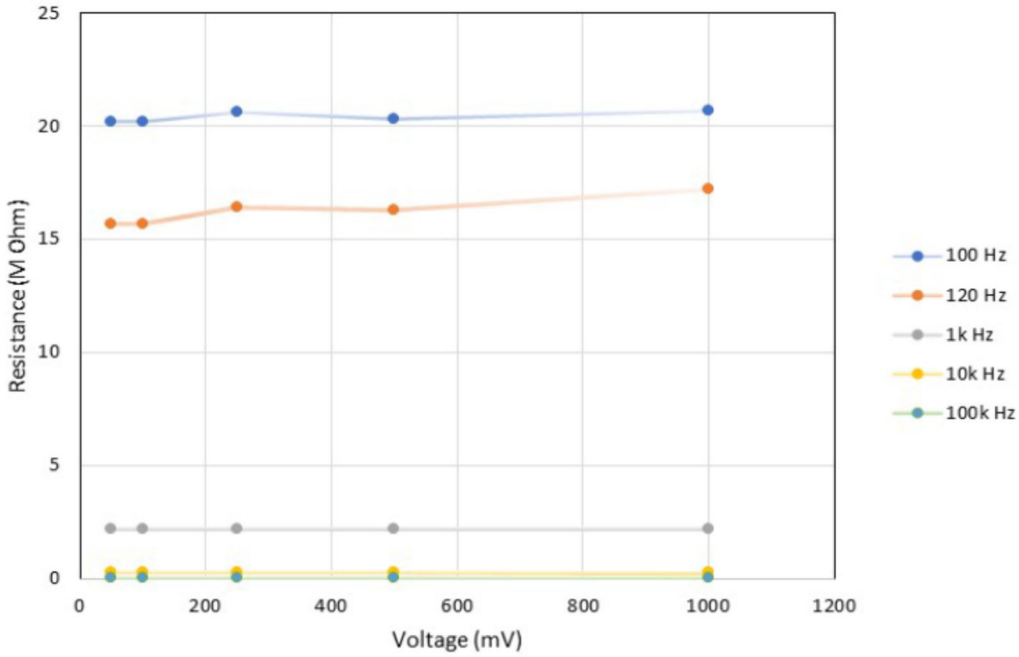

(b)

Fig. 9—(*a*) Resistance of PCTO ceramic processed at 900 °C and (*b*) PCTO ceramic processed at 1000 °C for identical size parallel pellets.

increase of capacitance and reduction of resistance. Contrary to this lower copper concentration in grains in PCTO processed at 900 °C shows higher resistivity and lower capacitance. Also, experimental data in this study at different frequencies showed that bulk dielectric constant reduces as the function of frequency which is a typical behavior of IBLC structure as shown by Sinclair *et al.*[7] The explanation of the theory that grain boundaries have intrinsic properties for high dielectric constant is valid in this case for the materials processed at these two temperatures for the PCTO system. As a function of frequency both parameters showed a decrease in magnitude of capacitance and resistance similar to commercial dielectric materials. Another major finding about this material system was that values of capacitance and resistance were totally unchanged as function of bias voltage. This is a strong signal that material does not show signs of deterioration due to

breakdown with applied bias. Overall data show that for higher dielectric constant materials should be processed at high temperature since copper depletes from the boundaries to grains into semiconducting grains. However, due to high content of copper the resistivity of the composite decreases.

IV. SUMMARY

We experimented to understand the transition of the morphological and the role of anisotropy on the morphology of the $Pr_{2/3}Cu_3Ti_4O_{12}$ (PCTO) material system processed at two different temperatures. The evolution and sizes of spherical and distorted grains altered to face complex shapes at high temperature (> 1000 °C) processing due to changes in the concentration of copper which alters the surface energy anisotropy. The grain growth appears to occur by the surface attachment/detachment rate and channel formations in the materials processed at lower temperatures (900 °C). Microstructures developed at high magnifications showed that new layers grew by screw dislocation mechanism. It indicates that the initial grain growth occurs by necking and channeling which enhances the coarsening. The transient bimodal grain size distribution consisting of large, growing grains were observed. The size and shape of distorted spherical grains of PCTO completely altered to faceted shape of grains which became asymmetrical as the growth progressed and the size of grains became larger. Microstructure showed that new layers on facets grew by screw dislocation mechanism suggesting that nucleation limited coarsening is occurring by the development of a transient bimodal growing grains with step. Very complex shaped grains grew in the metastable shapes and require further studies. Data show that for achieving higher resistivity, processing materials at low temperatures is beneficial.

ACKNOWLEDGMENTS

We are grateful and would like to acknowledge the support of the Biological and Physical Science Division, Science Mission Directorate, and the contribution of the Technical Lead for providing crystals grown at the NASA Marshall Space Flight Center and his active technical participation was extremely valuable. The authors are also grateful to the Program and Management Team of NASA, Marshall Space Flight Center Huntsville, for the technical input and discussion during this study.

CONFLICT OF INTEREST

There are no conflicts of interest that exist for all authors.

OPEN ACCESS

REFERENCES

1. M.A. Subramanian, L. Dong, N. Duanand, and B.A. Reisner: *J. Solid State Chem.*, 2000, vol. 151, pp. 323–25. https://doi.org/10.1006/jssc.2000.8703.
2. V. Kumar, S. Pandey, S. Singh, M.K. Verma, A. Kumar, N.B. Singh, and K.D. Mandal: *J. Aust. Ceram. Soc.*, 2000, vol. 56, pp. 1301–07. https://doi.org/10.1007/s41779-020-00469-x.
3. R.N. Singh: *J. Feroelectr.*, 2023, vol. 611(1), pp. 255–67. https://doi.org/10.1080/00150193.2023.2201788.
4. L. Singh, U.S. Rai, K.D. Mandal, and N.B. Singh: *Prog. Cryst. Growth Charact. Mater.*, 2014, vol. 60, pp. 15–62. https://doi.org/10.1016/j.pcrysgrow.2014.04.001.
5. R. Schmidt, M.C. Stennett, N.C. Hyatt, J. Pokorny, J. Prado-Gonjal, M. Li, and D.C. Sinclair: *J. Eur. Ceram. Soc.*, 2012, vol. 32(2), pp. 3313–23. https://doi.org/10.1016/j.jeurceramsoc.2012.03.040.
6. M.-W.-R. McKenzie, W. Zurawsky, and J. Mijovic: *J. Non-Cryst. Solids*, 2014, vol. 406, pp. 11–12. https://doi.org/10.1016/j.jnoncrysol.2014.09.035.
7. S.I.R. Costa, M. Li, J.R. Frade, and D.C. Sinclair: *RSC Adv.*, 2013, vol. 3, pp. 7030–36. https://doi.org/10.1039/c3ra40216a.
8. A. Deschanvres, B. Raveau, and F. Tollemer: *Bull. Soc. Chim. Fr.*, 1967, vol. 11, pp. 4077–80. https://doi.org/10.1016/0022-4596(79)90235-4.
9. B. Bochu, M.N. Deschizeaux, J.C. Joubert, A. Collomb, J. Chenavas, and M. Marezio: *Solid State Chem.*, 1979, vol. 29, pp. 291–94. https://doi.org/10.1016/0022-4596(79)90235-4.
10. J. Cai, Y.H. Lin, B. Cheng, C.W. Nan, J. He, Y. Wu, J. He, Y. Yu, and X. Chen: *Appl. Phys. Lett.*, 2007, vol. 91, pp. 252905–13. https://doi.org/10.1063/1.2825472.
11. K.D. Mandal, A.K. Rai, D. Kumar, and O. Parkash: *J. Alloys Compd.*, 2009, vol. 478, pp. 771–76. https://doi.org/10.1016/j.jallcom.2008.12.007.

12. S. Suresh, P.S. Vindhya, S. Devika, and V.T. Kavitha: *Mater. Today*, 2003, vol. 36, pp. 106657–59. https://doi.org/10.1016/j.mtcomm.2023.106657.
13. V. Kumar, S. Pandey, M.K. Verma, S. Singh, V.S. Rai, D. Prajapati, N.B. Singh, C.L. Prajapat, A. Gangwar, and K.D. Mandal: *J. Aust. Ceram. Soc.*, 2022, vol. 58, pp. 637–44. https://doi.org/10.1007/s41779-022-00724-3.
14. V.S. Rai, D. Prajapati, V. Kumar, M.K. Verma, S. Pandey, T. Das, N.B. Singh, and K.D. Mandal: *J. Mater. Sci. Mater. Electron.*, 2022, vol. 33, pp. 5273–82. https://doi.org/10.1007/s10854-022-07715-x.
15. A. Kumar, S.S. Yadava, L. Singh, M.K. Verma, N.B. Singh, and K.D. Mandal: *J. Magn. Magn. Mater.*, 2021, vol. 527, pp. 167807–15. https://doi.org/10.1016/j.jmmm.2021.167807.
16. V. Razdan, A. Singh, B. Arnold, F.-S. Choa, L. Kelly, and N.B. Singh: *Proceedings of SPIE 9493, Energy Harvesting and Storage: Materials, Devices, and Applications VI*, 18 May 2015, p. 949308. https://doi.org/10.1117/12.2177694.
17. J. Sebalda, S. Krohnsa, P. Lunkenheimera, S.G. Ebbinghausb, S. Rieggc, A. Rellerc, and A. Loidla: *J. Solid State Commun.*, 2010, vol. 150(17–18), pp. 857–60. https://doi.org/10.1016/j.ssc.2010.02.006.
18. N.B. Singh, J.J. Talvacchio, M. Sherwin, A. Berghmans, D.J. Knuteson, D. Kahler, B. Wagner, and J.D. Adam: *High Dielectric Capacitor Materials and Method of Their Production*, Northrop Grumman Systems Corporation, 2008, US20080218940-A1.
19. N.B. Singh, M. Gillan, D. House, R. Yanamaddi, and B. Arnold: *J. Emerg. Mater. Res.*, 2013, vol. 2(6), pp. 344–47. https://doi.org/10.1680/emr.13.00011.
20. N.B. Singh, A. Berghmans, M. King, M.D. Knuteson, J. Talvacchio, D. Kahler, M. House, B. Schreib, B. Wagner, and S. McLaughlin: *Cryst. Res. Technol.*, 2013, vol. 18(11), pp. 983–88. https://doi.org/10.1002/crat.v48.11.
21. L. Singh, U.S. Rai, K.D. Mandal, and N.B. Singh: *J. Nanosci. Technol.*, 2014, vol. 1(1), pp. 1–17.
22. M. Brandt, M. Kazmi, C.H. Su, N. Prasad, B. Arnold, F.-S. Choa, B. Cullum, E. Bowman, K. Machuga, and N. Singh: *Proceedings: Smart Biomedical and Physiological Sensor Technology XX*, 2023, vol. 12548, p. 1254804. https://doi.org/10.1117/12.2661233.
23. N.B. Singh, B. Schreib, M. Devilbiss, J. Loiacono, B. Arnold, F.-S. Choa, and K.D. Mandal: *Proceedings of SPIE 9865, Energy Harvesting and Storage: Proceedings of SPIE 9865, Materials, Devices, and Applications VII*, 13 July 2016, p. 986509. https://doi.org/10.1117/12.2220059.
24. T. Sano: Ph.D. Thesis on Interface Anisotropy and Its Effect on Microstructural Evolution During Coarsening, Materials Science and Engineering Department, Carnegie Mellon University, Pittsburgh, 2005.
25. N.B. Singh and M.E. Glicksman: *J. Cryst. Growth*, 1989, vol. 98, pp. 277–80. https://doi.org/10.1016/0022-0248(89)90142-5.
26. G. Wulff: *Z. Kristallogr.*, 1901, vol. 34, pp. 449–530.
27. C. Herring: *Phys. Rev.*, 1951, vol. 82(1), pp. 87–93. https://doi.org/10.1103/PhysRev.82.87.
28. M. Lifshitz and V.V. Slyozov: *J. Phys. Chem. Solids*, 1961, vol. 19, pp. 35–50. https://doi.org/10.1016/0022-3697(61)90054-3.
29. C. Wagner: *Z. Elektrochem. Ber. Bunsenges. phys. Chem.*, 1961, vol. 65(7–8), pp. 581–91. https://doi.org/10.1002/bbpc.19610650704.
30. P.W. Voorhees and M.E. Glicksman: *Acta Metall.*, 1984, vol. 32(11), pp. 2001–11. https://doi.org/10.1016/0001-6160(84)90181-0.
31. G.J. Shiflet, H.I. Aaronson, and T.H. Courtney: *Acta Metall.*, 1979, vol. 27(3), pp. 377–85. https://doi.org/10.1016/0001-6160(79)90030-0.
32. K. McReynolds, K. Wu, and P.W. Voorhees: *Acta Mater.*, 2016, vol. 120, pp. 264–72. https://doi.org/10.1016/j.actamat.2016.08.0562016.
33. K. Kim and P.W. Voorhees: *Acta Mater.*, 2018, vol. 152, pp. 327–37. https://doi.org/10.1016/j.actamat.2018.04.041.
34. V.A. Snyder, J. Alkemper, and P.W. Voorhees: *Acta Mater.*, 2001, vol. 49, pp. 699–709. https://doi.org/10.1016/S1359-6454(00)00342-6.
35. I. Seyhan, L. Ratke, W. Bender, and P.W. Voorhees: *Metall. Mater. Trans. A*, 1996, vol. 27A, pp. 2470–78. https://doi.org/10.1007/BF02652341.
36. F. Chadwick and P.W. Voorhees: *Acta Mater.*, 2021, vol. 205, pp. 116562–69. https://doi.org/10.1016/j.actamat.2021.116862.